Journal of Building Engineering 80 (2023) 108137

Contents lists available at ScienceDirect

Journal of Building Engineering

journal homepage: www.elsevier.com/locate/jobe

Durability tests on lime-based mortars from the historic built heritage of Catania (Eastern Sicily, Italy): An experimental study

Cristina Maria Belfiore [a], Giada Montalto [a], Claudio Finocchiaro [a,*], Giuseppe Cultrone [b], Paolo Mazzoleni [a]

[a] Department of Biological Geological and Environmental Sciences, University of Catania, Corso Italia 57, 95129, Catania, Italy
[b] Department of Mineralogy and Petrology, University of Granada, Avda. Fuentenueva, s/n, 18002, Granada, Spain

ARTICLE INFO

Keywords:
Historic mortars
Pore structure
Salt crystallization
Decay by SO_2
Durability

ABSTRACT

Mortars, like any other natural and artificial stone materials, are subject to atmospheric weathering agents which affect their durability according to the intrinsic characteristics of the material, such as mineralogical composition, texture and pore structure.

This paper aims to investigate the physical-chemical durability of lime-based mortars made with two different volcanic aggregates, locally known as *azolo* and *ghiara*, peculiar of the historic built heritage of Catania (Eastern Sicily, Italy). An experimental approach has been used, based on the reproduction in laboratory of historic mortars by using ancient recipes. The experimental samples have been characterized from a physical point of view and then subject to accelerated aging tests. Specifically, the samples have undergone: i) mineralogical investigations through X-ray diffraction (XRD); ii) thin section analysis by polarized optical microscopy; iii) pore structure analysis through mercury intrusion porosimetry (MIP); iii) water absorption by capillarity; iii) water vapor permeability test; iv) accelerated aging test by salt crystallization; v) decay by sulfur dioxide.

Results obtained highlight that the higher microporosity which characterizes the ghiara mortars is certainly responsible for their greater water absorption by capillarity as well as for their lower resistance to salt crystallization and exposure to sulfur dioxide, with respect to azolo-based ones.

1. Introduction

The materials used in the built heritage of a city are generally conditioned by the ease of supply of raw materials and therefore they depend on the specific geo-resources available in the surrounding area [1–9].

In the case of Catania, one of the greatest examples of Baroque architecture in eastern Sicily (Italy), the choice of construction materials is certainly conditioned by the presence of Mt. Etna volcano which, with its eruptive products, offers natural resources suitable for building. The peculiarity of the Catania Baroque lies, in fact, in the use of black lava stone which, combined with whitish calcareous lithotypes of the Hyblean area, give the buildings a peculiar bichromatic appearance [7].

The Baroque built heritage of the historic center of Catania is the result of the city reconstruction after two crucial natural events occurred during the second half of 17th century. The first one was the eruption of 1669, which took place on the southern flank of Mt.

* Corresponding author.
E-mail address: claudio.finocchiaro@unict.it (C. Finocchiaro).

https://doi.org/10.1016/j.jobe.2023.108137
Received 4 August 2023; Received in revised form 30 October 2023; Accepted 10 November 2023
Available online 14 November 2023

Etna volcano and lasted three months. The lava flow covered the densely populated areas of the Catania countryside, crossing the city and reaching the sea, erasing numerous villages and invading the cultivated areas [10]. A second major event was the earthquake occurred in 1693, the largest catastrophic event that affected eastern Sicily in historical times, causing the destruction of over 45 inhabited centers [11].

Over time, volcanic materials have been used in Catania both as building blocks and as aggregates in lime mortars. In the latter, two different materials typical of the Etna territory can be found, namely *azolo* and *ghiara*. Azolo, now obtained from the fine grinding of basalts, in its ancient meaning, was an incoherent pyroclastic rock with sharp edges and dark-gray color [12]. Instead, ghiara is a reddish material deriving from the thermal transformation at highly oxidizing conditions of paleo-soils, originally rich in organic matter, induced by lava flows. Both azolo and ghiara were used as aggregates in lime mortars during the intense reconstructive activity of the city in the 18th and 19th centuries. However, due to their better mechanical qualities as well as for the pleasant chromatic matching with the other construction materials, the use of ghiara mortars was further increased in the second half of the 18th century [13]. The lime mortars with volcanic aggregates remained in use until the mid-twentieth century, when they were replaced by modern cement mortars [14].

In situ surveys of the two types of mortars used in the historic built heritage of Catania show degradation phenomena which seem to affect more intensely those made with ghiara. The weathering forms commonly observed include salt efflorescence, chromatic alteration, disaggregation and detachment. Some examples of azolo and ghiara mortars, as well as the corresponding degradation forms, are shown in Fig. 1.

An important comparison study on these two types of lime mortars is represented by "Le malte del centro storico di Catania" (“The mortars of the historic center of Catania”) [14]. Here, the author provided information on azolo and ghiara mortars to understand and decode traditional building technology. He also gave technical indications in order to allow faithful restoration, to ensure, when possible, a continuity between the original material and the restoration one.

Later studies focused exclusively on the ghiara mortars to analyze the textural and compositional characteristics responsible for

Fig. 1. Examples of use of azolo (a–b) and ghiara (c–d) mortars in buildings of the historical city center of Catania and corresponding degradation forms: a) Palazzo Tezzano, built in the first half of the 18th century, and b) detail of salt efflorescence on the main façade and detachment of the outer layer; c) Esedra in Dante square, built in the second half of the 18th century, and d) detail of disaggregation and detachment of mortar portions from the main façade.

their pozzolanic behavior [15] or to define the chemical and mineralogical composition of the ghiara aggregates to shed light on its origin [16]. Other researches dealt exclusively with azolo, in particular with the use of these deposits (considered to be natural waste material by national legislation) for the production of alkaline activated binders and mortars [17]. Only recently, Belfiore et al. [12] focused on both azolo- and ghiara-based lime mortars highlighting and quantifying their hydraulic behavior in terms of reactivity between binder and aggregates. Specifically, through an innovative semi-automated image processing procedure based on the multivariate statistical analysis of X-ray maps, the authors mapped the distribution of the Hydraulicity Index (HI) in both mortars. They found that HI is quite higher in the ghiara mortar with respect to the azolo one and this is because azolo is almost inert when mixed with the slaked lime, showing low reactivity in the hardening process of the mortar; conversely, ghiara is a chemically reactive material since it contains silicates and aluminates which at room temperature and in presence of water react with the calcium hydroxide to form hydrated silicates, which are responsible for the better hydraulic properties of ghiara mortars (Belfiore et al. [12]).

The mechanical resistance of ghiara and azolo lime-based mortars has already been tested by previous authors [14] who highlighted better performance for the ghiara-made mortars. This is certainly due to their higher hydraulicity, whose effects on the compressive strength depend on both the porosity and the carbonation process (in lime mortars, progressive carbonation increases the strength and decreases porosity) [18]. Conversely, as regards their durability, i.e., the ability of a material to withstand mechanical, physical and chemical degradation processes in full compliance of its design functionality [19], no studies in the existing literature have tested the decay resistance of these two mortars and this is the purpose of our research. Notoriously, the durability of a material is strongly influenced by a number of factors including: a) the local environmental conditions (e.g., air pollution, acid rain, frost, thermal dilation, wetting-drying, wind weathering and biological attack); b) the ingredients used for the mortar preparation and the relative proportions (e.g., binder, aggregates and water), which also influence the pore network; and c) on-site construction practices [20]. Several studies in literature have dealt with historical lime-based mortars with volcanic aggregates, mostly focusing on their characterization from a mineralogical-petrographic and chemical point of view [21–24]. Instead, researches regarding their durability, through the reproduction in laboratory of replicate mortar specimens with compositionally similar aggregates, are almost missing in literature. Regarding the testing methodologies to estimate mortar durability, the most commonly used include wetting-drying cycles, freeze-thaw cycling and salt crystallization damage tests [20,25–28].

In our case study, the durability assessment of ghiara and azolo mortars has been carried out on laboratory replicas through those accelerated aging tests which most closely simulate the real causes of degradation (i.e, salt crystallization and exposure to sulfur dioxide). Indeed, the main causes of stone decay in the historic center of Catania are related to salts from both capillary rising and marine spray (Catania is a seaside city), urban pollution and volcanic gas emissions from Mt. Etna.

2. Raw materials and preparation of lime-based mortar test specimens

For the preparation of mortar samples, a ready-made commercial slaked lime supplied by La Nuova Fornaciaia s.r.l. (Italy) was used as binder. It consists of calcium hydroxide, classified as CL80-S PL (according to EN 459-1: 2015 [29]), with a semi-solid consistency, density 1290 kg/m^3, CaO content >90%, MgO content 1.5–2% and solid/water ratio 40:60. As for the volcanic aggregates, ghiara samples were collected at Cava Perniciano, an ancient quarry associated to the lava flow of 1669 and located near the town of Belpasso, in the province of Catania, while regarding azolo, prepackaged bags, supplied by La Rosa & Magrì snc (Catania, Italy), were purchased. Both azolo and ghiara aggregates, from a morphological viewpoint, appear to be sub-rounded to angular and with high sphericity.

The historical mortars were reproduced in the laboratory by using the ancient recipes known from literature [14,30]. In particular, the binder/aggregate ratio per volume was 1:2. Before preparing this mixture, both aggregates underwent granulometric separation by sieving. Out of 1 kg of aggregate, the proper amount of each size class to be added in the mixture was calculated through the Fuller's particle size equation (Table 1). The maximum grain size used for the aggregates is 2 mm since such experimental mortars are thought for finishing purposes.

For the mortars' preparation, a mixer was used to homogenize the mixture. During this step, a certain amount of water (~3 vol% in the ghiara mortar and ~5 vol% in the azolo one) was also added for achieving adequate workability. Finally, the mixture obtained was poured into 5x5x5 cm molds and placed on a vibrating table to improve the packaging by removing air bubbles. A total of 48 test samples was produced, 24 of azolo-based mortars (labeled as CA) and 24 of ghiara-based mortars (labeled as CG), which were then removed from the molds after 7 days and left curing for further 21 days at room temperature in laboratory (25 °C and 80–85% relative humidity). After demoulding, the specimens exhibited some imperfections in their macroscopic appearance, such as rough surface, lack of straight edges (generally more evident in the azolo mortar specimens), and presence of some microcracks due to the shrinkage during curing process. In addition, the upper surface of specimens appeared to be whitened due to its contact with the air during the first seven days of curing in the molds, favoring the carbonation process.

Table 1
Amount of each grain size class per kg of aggregate used for the preparation of mortars, calculated through the Fuller's equation.

Grain size class (mm)	Amount (g)/1000g of aggregate
1–2	356
0.500–1	252
0.250–0.500	178
0.125–0.250	126
0.063–0.125	88

3. Methods

To ascertain the mineralogical-petrographic and physical characteristics of the designed mortars as well as their durability, the samples underwent the following laboratory investigations after 28 days of curing.

The mineralogical analysis of both aggregates (azolo and ghiara) and mortars was performed through a Rigaku Miniflex X-ray diffractometer (XRD). X-ray diffraction patterns were acquired in the range 5°–70° 2θ, using a step-size of 0.02° and a step-time of 5 s. Phase identification was performed through QualX software [31].

The thin section analysis of mortars has been carried out on a Leika ICC50W polarizing microscope (equipped with digital camera to capture images) to investigate the textural features of the two laboratory mortars also in comparison with the historic ones from monuments of Catania.

The pore system of mortar samples within a range of 0.005–750 μm was analyzed by mercury intrusion porosimetry (MIP) using a Micromeritics Autopore V 9600 porosimeter reaching a maximum pressure of 227 MPa. Open porosity (P_o, %), specific surface area (SSA, m^2/g) and apparent and real densities (ρ_a and ρ_r, g/cm^3) were calculated on mortar samples.

The water absorption by capillarity was determined according to the European standard UNI EN 1015-18 (2004) [32]. Three specimens per each mortar type were placed inside a ventilated oven for 24 h to remove residual moisture and after that the dry weight of each sample was calculated. Then, the specimens were placed inside a container with the lower face immersed in about 5–10 mm of water and covered to prevent water evaporation. After 10 min, the specimens were extracted from the basin and weighted (M_1), then again immersed and after 90 min weighted to obtain the final mass (M_2). The capillary coefficient was calculated through the following formula (Eq. (1)):

$$C = 0.1(M_2 - M_1)\ kg \,/\, \left(m^2 \bullet min^{0.5}\right) \tag{1}$$

The amount of absorbed water (Q_i) was calculated as follows (Eq. (2)):

$$Q_i = (w_i - w_0)/A \tag{2}$$

where: w_i and w_0 are the weights (in g) of the sample at times t_i and t_0, respectively; A (cm^2) is the area of the surface exposed to water.

The water vapor permeability test was carried out on four samples for each mortar type with a prismatic shape of 5 × 5 × 1 cm. The equipment consisted of a test tube filled with 25 ml of deionized water, which was screwed to a cap previously sealed with silicone to the lower face of the sample (avoiding its contact with the water). The entire equipment, consisting of the mortar specimen plus the cylinder containing the water, was weighted a first time before the beginning of the test and then again after 8 h, 24 h, 48 h, 72 h and 96 h. The weight decrease (as a function of the sample thickness) over time was a function of water vapor permeability of investigated specimens.

The studied mortars also underwent accelerated aging tests to simulate in laboratory conditions the degradation processes to which they are subject when exposed in outdoor environment. In particular, the resistance of mortar samples to salt crystallization and their behavior when exposed to sulfur dioxide (SO_2) were tested. The salt crystallization test was carried out according to the UNI EN 12370 (2020) standard [33]. The samples underwent fifteen 2 h-cycles at 20 °C of total immersion in a 14% $Na_2SO_4 \times 10H_2O$ solution and subsequent drying for 16 h at 105 °C. After the 15th cycle, the samples were placed in deionized water for 24 h to dissolve any sodium sulphate retained in pores and fissures of mortars, then rinsed with running water, put in the oven and weighed to obtain the final mass (M_f) compared to the initial dry mass (M_d). The results were expressed as percentage weight loss (ΔM%) through the following equation (Eq. (3)):

$$\Delta M = \frac{M_f - M_d}{M_d} \bullet 100 \tag{3}$$

After the salt crystallization test, MIP analysis was carried out on the degraded samples to investigate the modifications undergone by the pore structure.

An accelerated decay test by sulfur dioxide (SO_2) was also carried out to simulate the action of natural (volcanic) and anthropic air pollution. Due to the inadequacy of current standards to simulate this type of test, some authors have suggested modifications to the procedures, proposing experimental conditions more suitable for reproducing the degradation processes of stone materials in the laboratory [34–37]. The procedure carried out here is the one followed by Fioretti (2016) [38], which involved the use of a hermetically resealable vacuum bell, connected to a vacuum pump on one side and to a conical flask on the other through silicone tubes and closing valves. The test samples, three for each type of mortar were placed on a perforated grid, in the lower hemisphere of the bell. Then, 100 ml of sodium sulphite dissolved in water was introduced into the bottom of the bell through a thin glass funnel. At the end of this first phase, the bell was sealed with vacuum grease. The vacuum pump, previously connected to the bell by means of a small tube, was then operated and, once the vacuum was reached, it was turned off. At that time, 110 ml of hydrochloric acid dissolved in the distilled water was introduced by a small tube connecting it to the bell. When the transfer of the solution was completed, the connecting valve with the flask was closed to prevent air from entering. At the end of this operation, the production of sulfur dioxide took place, so giving start to the exposure of the samples, which were kept in the system saturated with SO_2 for 30 days.

To investigate any physical and compositional changes occurred on the surface of the samples at the end of the SO_2 treatment with sulfur dioxide, colorimetric analysis, mineralogical and morphological/chemical investigations were carried out. Specifically, the colorimetric measurements were performed by using a portable Konica Minolta CM-2600d spectrophotometer on both degraded and unaltered samples to assess the possible color changes at the end of the test. All measurements were made in D65 illuminant, diameter of measuring window 8 mm and 10-degree viewing angle. Three measurements were carried out on each of three faces of the sample.

This test allows an accurate measurement of the color of the object through the acquisition of L*, which indicates the lightness, together with a* and b*, which represent the chromatic coordinates. To quantify the color change of degraded samples compared to the unaltered ones, the ΔE value was calculated according to the following formula (Eq. 4):

$$\Delta E = \sqrt{\left(L_2^* - L_1^*\right)^2 + \left(a_2^* - a_1^*\right)^2 + \left(b_2^* - b_1^*\right)^2} \quad (4)$$

The mineralogical analysis of secondary phases developed on the samples' surfaces after the SO_2 treatment was performed through XRD directly on the surface of mortars' fragments by using the same setting conditions described above. Morphological and chemical investigations have been carried out on degraded samples through a scanning electron microscope (model TESCAN VEGA), equipped with Energy-dispersive X-ray spectroscopy, EDS Neptune XM460 series, at an accelerating voltage of 20 kV and a beam current of 0.2 nA.

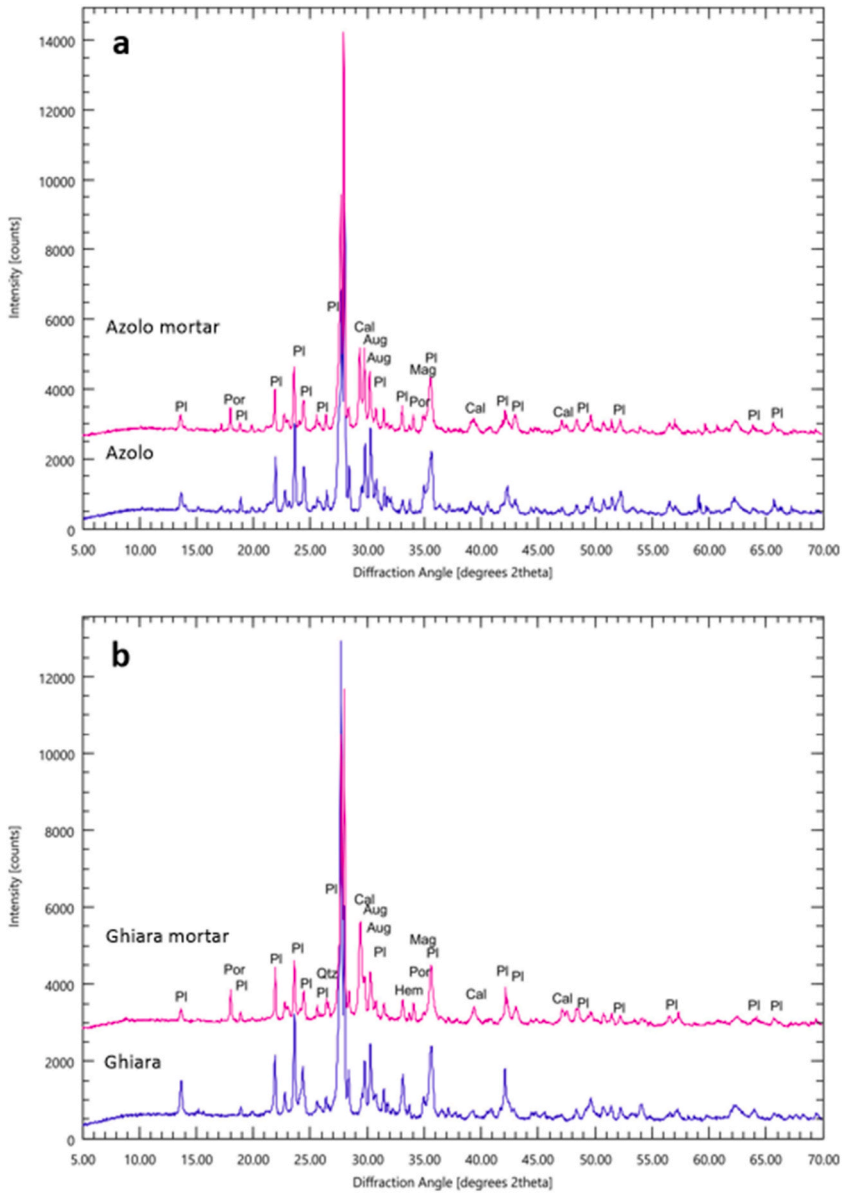

Fig. 2. XRD patterns of: a) azolo (blue) and azolo-based mortar (magenta); b) ghiara (blue) and ghiara-based mortar (magenta). Pl = plagioclase, Aug = augite, Mag = magnetite, Hem = hematite, Cal = calcite, and Por = portlandite.

4. Results and discussion

4.1. X-ray diffraction analysis

The mineralogical composition of the designed mortars was determined after 28 days curing. The data were then compared with the mineralogical composition of the aggregates used for the two mortar types. The phases occurring in the azolo aggregate (Fig. 2a) include plagioclase, augite and magnetite. The XRD pattern of the mortar made with azolo aggregates shows the same minerals with in addition calcite and low amounts of portlandite, while there are no evidences of CSH/CAH phases. The same results are visible in the diffractograms of ghiara and ghiara-made mortars (Fig. 2b), where, in addition to the above-mentioned phases, hematite and quartz are also observed. Hematite is related to the transformation processes of the palaeo-soil by the lava flow, while quartz is due to epiclastic contribution [15]. The lack of hydraulic phases in azolo mortars is consistent with the literature [12] according to which such materials have poor hydraulic properties due to a low reactivity of azolo with lime. Conversely, the absence of CSH and CAH phases in the ghiara mortar seems to be in contrast with what has been previously observed by other authors [12,15,39], who highlighted for these mortars hydraulic properties comparable to those of pozzolana. Therefore, this result could be due to the intrinsic limitations of the technique used. Indeed, as known, XRD is not fully performing in the identification of CSH and CAH phases, since most of these are poorly crystalline and, in most cases, occur in small amounts, often lower than the detection limit of the technique [12,40–42]. Alternatively, the absence of hydraulic phases in the diffraction patterns of the two mortars could be due to the preparation and curing conditions of the samples.

4.2. Thin section analysis

Optical microscopy observations highlight that though the aggregates of the two mortar types are both of volcanic nature and with the same mineralogical assemblages, they are characterized by some different textural features, as previously found by Belfiore et al., 2022 [12]. In particular, the azolo mortar (Fig. 3a) mainly exhibits an aggregate/binder ratio of about 60/40. The binder is quite homogeneous, with a micritic texture and greyish color. The porosity is mainly of secondary type and consists of microcracks due to shrinkage. The aggregates, with grain size in the range of 0.063 μm–2 mm, have a polymodal distribution and a moderate sorting, according to Fuller's equation. From a compositional point of view, they include both rock fragments and single crystals given by plagioclase, as the most abundant phase, followed by clinopyroxene, olivine and Fe–Ti-oxides. The rock fragments, from sub-rounded to sub-angular, generally exhibit porphyritic structure with phenocrysts of the same phases above mentioned and a prevalently vitrophyric groundmass. Subordinate clasts with vesiculated textures can be also observed.

The ghiara mortar (Fig. 3b) exhibits an aggregate/binder ratio of about 60/40. The binder is light brown in color and shows a micritic texture. Even in this case, the porosity is mostly given by microcracks. The aggregate is formed by clasts with sizes ranging from 0.063 μm to 2 mm, polymodal distribution and sub-rounded to sub-angular shape. The coarser grains have the same textural and compositional features as those occurring in the azolo mortar but with a reddish-brown coating, while the finer clasts are entirely reddish-brown and optically isotropic. The single crystals of the aggregates consist of plagioclase, clinopyroxene, olivine, Fe–Ti-oxides

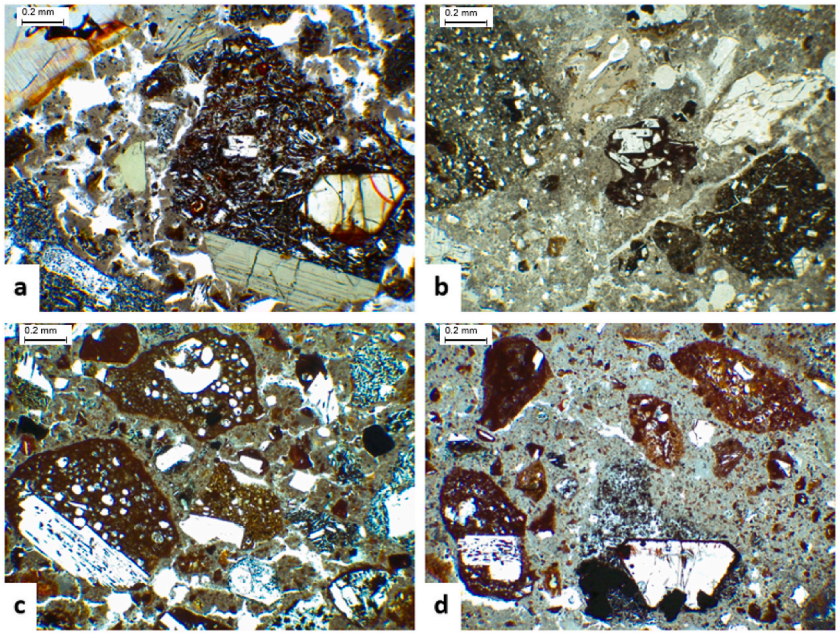

Fig. 3. Photomicrographs representative of: a) laboratory azolo mortar; b) historical azolo mortar from the Church of San Francesco Borgia in Catania; c) laboratory ghiara mortar; d) historical ghiara mortar from the external walls of the Benedictine Monastery in Catania. All photos have been taken at plane polarized light, objective 4x. Scale bar = 0.2 mm.

and quartz (the latter in small amount).

The comparison of the laboratory mortars examined with two historical ones from local monumental buildings of Catania [12] puts into evidence a strong similarity in terms of textural and compositional features, although the grain size of aggregates in the historical samples appears to be comprised in a wider range with clasts reaching 7 mm in the ghiara mortar and 3 mm in the azolo one. This difference can be certainly ascribed to the unlike intended use, since the reference mortars [12] were used for rendering aims thus needing coarser aggregates, while our laboratory mixtures were thought for finishing purposes.

4.3. Mercury intrusion porosimetry (MIP) analysis

The results regarding the specific surface area (SSA), the apparent and real densities (ρ_a and ρ_r), and the open porosity (P_o) of both mortar types determined by MIP are reported in Table 2. In detail, the two types of mortars are different in terms of SSA, which is higher in the samples with ghiara (>3 m^2/g) than in those with azolo (~1.6 m^2/g). This suggests the presence of smaller pores in CG samples. They are also the samples with the highest porosity (46.6% for ghiara mortars compared to 38.5% for the azolo ones). Overall, the values of accessible porosity found here fall into the range of other lime-based historical mortars from the Naples district (Italy) (38–52%) [21–23]. Regarding the density of the mortars, the apparent density is higher in the azolo samples (1.8 g/cm^3) than in the ghiara ones (1.6 g/cm^3). The real density (ρ_r) is almost the same in both types of mortars being $\cong$ 3 g/cm^3, considering that they have similar mineralogy.

The results of pore size distribution are plotted in Fig. 4. At first sight, all specimens of both sets display a general bimodal distribution with two main pore classes falling in the ranges 0.1–1 (typical of ancient hydraulic mortars [27]) and 10–100 μm, while a third minor pore class is located in the range 1–10 μm. Ghiara mortars (sample CG) display a higher and wider frequency in the range 0.01–1 μm, which justifies the higher SSA value measured in this sample set. The azolo mortars (sample CA) show a quite higher peak in the range 10–100 μm and slightly shifted to the right of the diagram (i.e., towards bigger pores).

4.4. Water absorption by capillarity

Notoriously, the water absorption of a mortar is strongly influenced not only by the type, size and porosity of aggregates, but also by the water amount used for the preparation of the mixture as well as by the final porosity of the mortar following the mixing and compaction for voids reduction [43]. The results of water absorption by capillarity are shown in Table 3, which lists the average values of C (water absorption coefficient) and Q_i (absorbed water amount) for each type of mortar. Fig. 5 shows the average trend of water absorption by capillarity for each mortar sample until 90 min from the beginning of the test. The most marked difference between the two mortars can be observed in the first section of the curve (from time t_0 to time t_{10}), where the average absorption coefficient of the ghiara mortars (C_{10}= 4.6 $kg/m^2min^{0.5}$) is double that of the azolo ones (C_{10}= 2.5 $kg/m^2min^{0.5}$). Conversely, in the second portion of the curve, from time t_{10} to time t_{90}, the trend is quite similar, though the average coefficient is slightly higher in the azolo samples (6.3 $kg/m^2min^{0.5}$ *vs*. 4.9 $kg/m^2min^{0.5}$). The adsorbed water at the end of the test (Q_i) is higher in the ghiara mortars (Q_i= 19.9 kg/m^2) than in the azolo ones (Q_i= 14.8 kg/m^2). The higher porosity which characterizes the ghiara mortars, as evidenced by MIP analysis, explain why they absorb more water and more rapidly than azolo mortars.

4.5. Water vapor permeability

With regard to water vapor permeability, the trend of the weight loss of the samples over time can be observed in the diagram of Fig. 6, where the azolo mortar samples record a slightly higher weight loss than the ghiara ones. In particular, at the end of the test, the azolo samples show an average weight loss of 8.9%, while those made with ghiara of 6.5%. Therefore, the results obtained seem to indicate that azolo mortars have a greater permeability to water vapor than the ghiara ones. However, by considering the curves of both samples analyzed for each mortar type in Fig. 6, a partial overlapping is observed or, in any case, the difference between the two mortars is negligible.

4.6. Accelerated aging test by salt crystallization

Generally, pozzolanic lime mortars are quite porous and permeable materials, allowing a significant amount of saline solution to enter in the porous network so facilitating the deterioration.

The salt crystallization test shows that, at the end of the fifteen cycles, the mortars exhibit a very important mass decrease, in particular the ghiara-based samples have an average mass loss of 63.55%, almost double that of the azolo ones ($\Delta M = 38.40\%$). From the curves in Fig. 7, which correlate the average mass variation of each mortar sample with the fifteen cycles, it can be observed that during the first cycle, both samples show a slight mass increase (1% in azolo mortars and 1.5% in ghiara ones) due to the crystallization of salts inside the pores. From the second cycle onwards, the azolo sample shows a regular trend, characterized by a constant and

Table 2
Results of MIP test. SSA = specific surface area; ρ_r = real density; ρ_a = apparent density; P_o = open porosity. CA and CA-S = azolo mortar before and after the salt crystallization test; CG and CG-S = ghiara mortar before and after the salt crystallization test.

	SSA (m^2/g)	ρ_r (g/cm^3)	ρ_a (g/cm^3)	P_o (%)
CA	1.57	2.99	1.84	38.5
CA-S	1.70	3.11	2.04	34.4
CG	4.23	3.04	1.62	46.6
CG-S	3.35	2.75	1.63	40.6

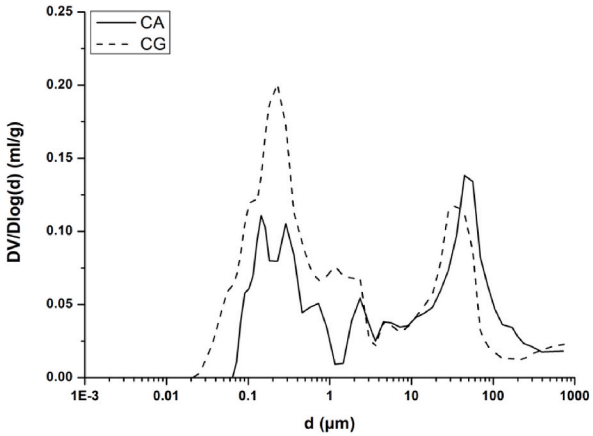

Fig. 4. MIP pore size distribution curves (log differential intruded volume in ml/g vs. pore diameter in μm) of unaltered azolo (CA)- and ghiara (CG)-based mortars.

Table 3
Results of the water absorption test by capillarity. $C_{(10\ min)}$ and $C_{(90\ min)}$ = absorption coefficient after 10 and 90 min from the beginning of the test; $Q_{i\ (90\ min)}$ = amount of absorbed water at the end of the test.

	$C_{(10\ min)}$ (Kg/m^2·min$^{0.5}$)	$C_{(90\ min)}$ (Kg/m^2·min$^{0.5}$)	$Q_{i\ (90\ min)}$ (Kg/m^2)
		Azolo mortar (CA)	
Average	2.47	6.28	14.83
St. dev.	*0.56*	*0.65*	*6.07*
		Ghiara mortar (CG)	
Average	4.59	4.86	19.94
St. dev.	*0.86*	*1.16*	*8.44*

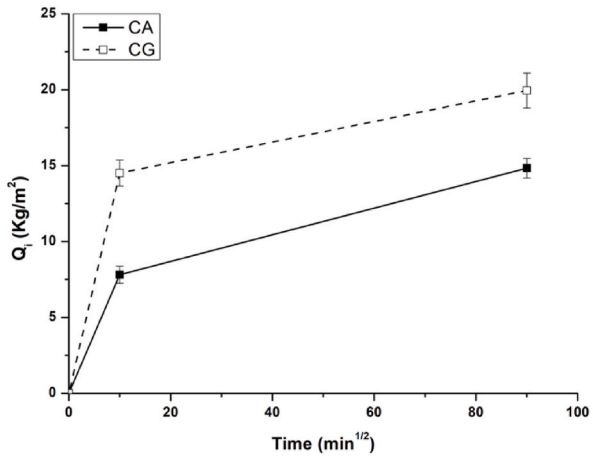

Fig. 5. Average curves of water absorption by capillarity in the two mortar types investigated.

gradual mass decrease, for the entire duration of the test. Conversely, the ghiara mortar displays a slight mass increase (1.8%) also in the second cycle, after that the mass starts decreasing (Fig. 7). In this case, the trend appears to be gradual up to the 7th cycle, while between the 7th and the 9th cycles, a more rapid decrease occurs and then the mass loss returns to be more gradual until the end of the test.

Overall, though our laboratory mortars at the end of the salt crystallization test evidence a significant decay, their behavior can be considered acceptable if compared to some other pozzolanic mortars which do not complete the entire test [44].

From a morphological viewpoint, all the specimens of azolo and ghiara mortars in the first five cycles keep almost intact their cubic shape, showing only a slight smoothing of corners and edges. From the sixth cycle onwards, the loss of material becomes increasingly evident, particularly in the ghiara mortars, up to the fifteenth cycle when the edges are totally lost and the morphology of the specimens is no longer recognizable (Figs. 8 and 9).

The much more considerable loss of material registered in the ghiara mortars may be related to their pore size distribution and, in

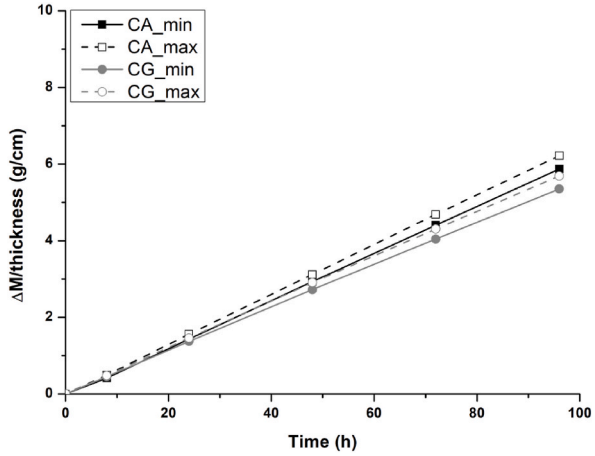

Fig. 6. Diagram showing the weight variation (ΔM) of ghiara (CG) and azolo (CA) mortars (as a function of their thickness) during the water vapor permeability test.

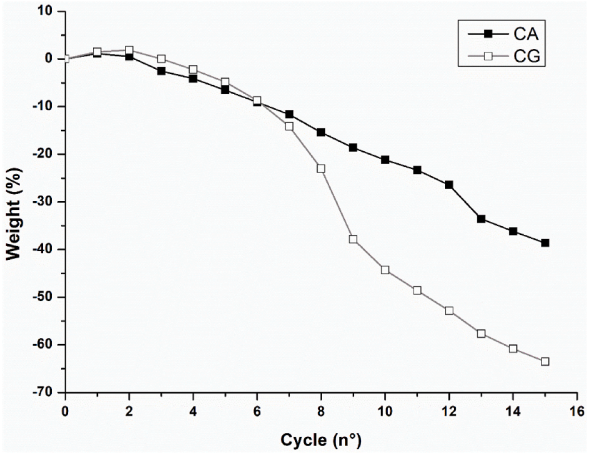

Fig. 7. Diagram showing the average trend of weight loss (ΔM%) of azolo (CA) and ghiara (CG) mortars during the crystallization cycles.

particular, to their higher microporosity with respect to azolo samples (see Fig. 4). As known, the smallest pores are the most harmful in terms of salt degradation as they are the ones mostly subject to crystallization pressures with consequent breakdown of the pore walls and disaggregation of the material [45].

The results obtained highlight that in this test, morphological imperfections and structural defects of the samples did not play an important role in determining the behavior to salt decay. Indeed, a greater degradation was expected for the azolo mortar samples that generally displayed the most evident imperfections, while, on the contrary, they recorded a significantly lower mass loss than the ghiara mortars.

The MIP analysis performed on the mortars after the salt crystallization test highlight that, in the case of azolo-based mortars, the main difference observed between degraded (CA-S) and unaltered (CA) samples consists in the reduction of peak frequency of pores in the range 1–10 μm and the appearance of a new pore cluster in the range 0.01–0.1 μm (Fig. 10a). Instead, the degraded ghiara mortars (CG-S) exhibit almost the same pore size distribution as the unaltered ones, though the salt crystallization reduces the frequency of pores in the range 0.1–1 μm (Fig. 10b). After the test, the open porosity slightly decreases in both samples (from 38.5% to 34.4% in the azolo mortars and from 46.6% to 40.6% in the ghiara ones, Table 2) due to the presence of some salt crystals, which remained trapped in the pore system of mortars. The slight increase of real density observed in the CA-S sample with respect to the CA one (though this difference is negligible), is probably due to a less effective washing after the aging test and therefore to a higher amount of sodium sulphate still present in pores and fissures of this sample or, alternatively, due to heterogeneity of the mortar. In the case of azolo mortar, the total pore volume is lower in the degraded sample with respect to the unaltered one, though the pore radius mode is shifted towards lower values (Fig. 10a), suggesting that some salt crystals obstruct pore entries. Even in the case of ghiara mortar, the total pore volume is lower in the degraded sample (Fig. 10b), however the pore size mode is almost the same for unaltered and degraded samples, thus indicating that salt crystals partially fill the pores. This different behaviour is well explained by the model proposed by Angeli et al., 2008 [46] and successively applied by Barone et al., 2015 [47], which refers to the monitoring cycle by cycle of the salt crystallization inside the pores to explain the degradation mechanisms of sedimentary rocks.

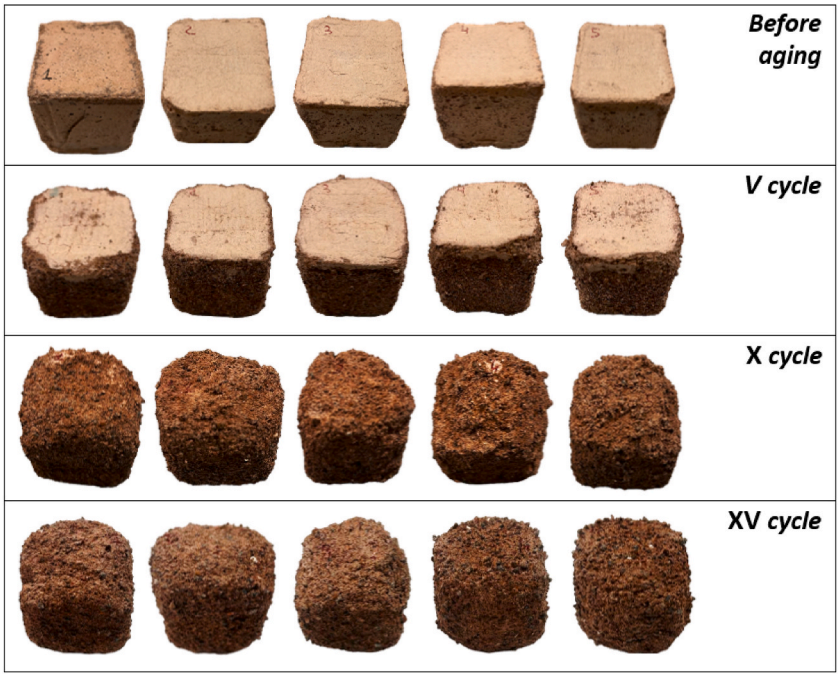

Fig. 8. Degradation of the ghiara-based specimens during the salt crystallization cycles.

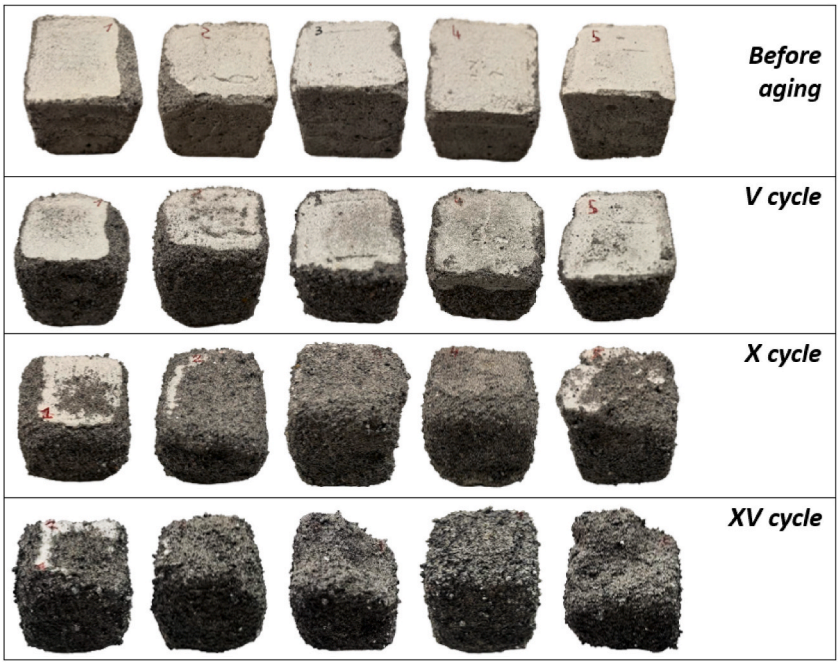

Fig. 9. Degradation of the azolo-based specimens during the salt crystallization cycles.

4.7. Decay by sulfur dioxide

Sulfur dioxide is the most dangerous among the gassy atmospheric pollutants. Its interaction with the mortars is a complex factor very difficult to be determined due to the many variables involved in the process (e.g., concentration of the gas in the atmosphere, direction of the wind, intensity of the rain, etc.). Furthermore, the effect of SO_2 on the mortar is a function of several intrinsic factors of the material such as nature of the binder, microstructure, porosity, permeability, etc. [48].

In our case study, at the end of 30 days sulfur dioxide test, the samples' surfaces exhibited color stains darker than the original one,

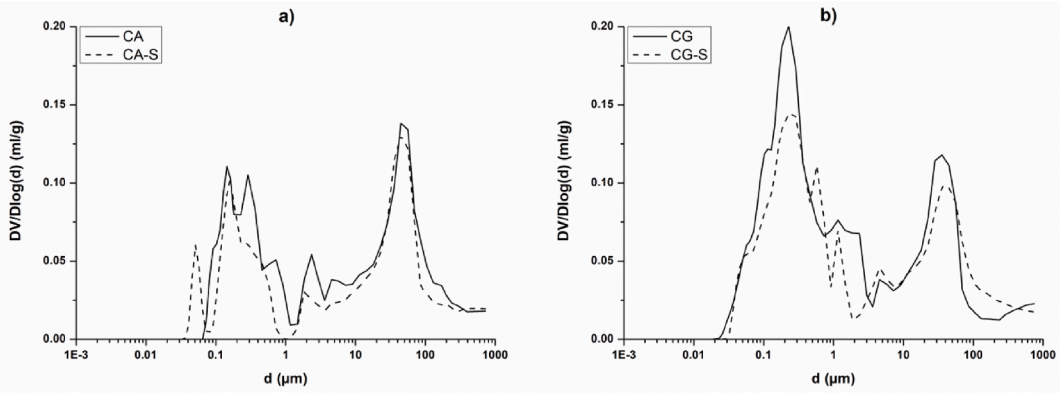

Fig. 10. MIP pore size distribution curves (log differential intruded volume (ml/g) vs. pore diameter (μm)): a) azolo-based mortar and b) ghiara-based mortar after the salt crystallization test (dashed lines, CA-S and CG-S), compared to the unaltered samples (straight lines, CA and CG).

which were mainly concentrated all near the edges (Fig. S1 – supplementary material). Such stains were much more widespread in the ghiara samples thus highlighting that the latter suffered a more intense SO_2 attack. This is probably due to the greater microporosity that characterizes the ghiara mortars compared to the azolo ones, as revealed by MIP analysis. It's worth noting that, contrary to the salt crystallization test where morphological imperfections and structural defects of the samples (such as lack of sharp edges, presence of microcracks, etc.) did not play an important role in determining the behavior to salt degradation, in this test such imperfections affected the response of the single sample to the SO_2 attack. Indeed, just the portions of the samples corresponding to the missing edges are those characterized by a more intense modification, even if with a greater extension in the ghiara mortars' specimens.

To better highlight the changes induced by sulfur dioxide, colorimetric analysis and SEM-EDS observations were performed on the surface of samples before and after the decay test by SO_2 contamination. The average values of L*, a* and b* parameters measured on unaltered and degraded azolo-based mortars showed a ΔE of 3.7 which, although falling within the range of noticeable color variation [49], is quite moderate (Table 4). Instead, the average ΔE calculated for the ghiara-based mortars is 7.7, which indicates an important chromaticity variation that is certainly visible to the naked eye.

Some authors stated that gypsum is the only stable salt formed during the interaction of SO_2 with hydraulic mortars, while others considered the possibility of formation of thaumasite and ettringite [48]. In our case, SEM observations allowed to identify the composition of the dark stains which resulted to be formed by minute gypsum crystals with prismatic or tabular shape (Fig. 11). These crystals form through the reaction between the calcium carbonate of the substrate, the sulfur dioxide and the water present in the system. One of the azolo-based specimens also showed the occurrence of fibrous crystals whose habit and composition, given by S, Ca and Al, can be attributed to ettringite formed by the reaction between the CAH phases of the mortar and the calcium sulphate [50]. The mineralogical nature of these newly-formed crystals due to the SO_2 attack was confirmed by the X-ray diffraction analysis performed directly on a fragment of the surface of both the dark and the light areas of the samples (Fig. 12). It is evident that, besides the primary phases such as plagioclase, augite, and calcite (along with hematite in the ghiara mortar) which are associated to the aggregate and binder components of the mortars, the dark areas of both specimens show very intense reflection peaks of gypsum (Fig. 12 a-b), along with small amounts of ettringite in the azolo mortar (Fig. 12a). In the XRD patterns of the light portions, these secondary phases display a considerably reduced intensity (Fig. 12 a-b).

5. Conclusions

Results obtained from XRD and thin section analysis of the designed mortars highlight similar mineralogical and textural features compared to the reference-historical ones from monumental buildings. The only differences observed regard: a) the lack of hydraulic phases in our laboratory mortars, contrarily to the historical ones (where these phases were identified and quantified by other authors through a GIS-based image processing approach), which is ascribable to intrinsic limitations of X-ray diffraction analysis or to the preparation and curing conditions; b) a finer grain size of aggregates in designed mortars with respect to the historical ones.

The physical characterization of the two laboratory mortars highlighted that the ghiara-based ones display higher porosity, particularly in the range of micropores, and this is certainly responsible for their major and more rapid water absorption by capillarity. Conversely, in the water vapor permeability test, the two mortars exhibit a similar behavior.

Accelerated aging tests have shown that azolo mortars display better performance in terms of degradation by sulfur dioxide and, above all, in terms of resistance to salt crystallization which, as known, is one of the main causes of degradation in porous materials. The mass loss recorded by the ghiara mortar samples after the salt crystallization test is, in fact, almost double that shown by the azolo mortars. This is certainly ascribable to the greater microporosity that characterizes the former and therefore to their greater water absorption by capillarity which leads to the migration of saline solution in the pore network of the samples. The salts exert a crystallization pressure on the pore walls, which accelerates weathering so lowering the durability. These results are consistent with the real degradation conditions of ghiara and azolo mortars when exposed in outdoor environment, since *in situ* observations highlight that the decay processes generally affect more intensely the ghiara-made mortars.

Table 4
Results of colour measurements carried out on the ghiara and azolo mortars before and after the decay by sulfur dioxide.

GHIARA MORTAR							
	Unaltered sample			Sample degraded by SO_2			
	L*	a*	b*	L*	a*	b*	ΔE
Max	68.7	11.6	14.9	56.8	14.8	17.3	12.3
Min	65.9	12.3	15.2	63.7	12.4	15.4	2.1
Average	70.9	11.1	14.2	63.7	12.4	14.5	7.7
St. dev.	3.7	1.2	1.2	5.6	1.7	2.1	3.5
AZOLO MORTAR							
	Unaltered sample			Sample degraded by SO_2			
	L*	a*	b*	L*	a*	b*	ΔE
Max	82.8	0.5	0.5	75.8	0.8	2.7	6.8
Min	83.4	0.5	0.2	81.7	0.4	0.8	1.8
Average	73.7	0.8	1.2	70.7	0.9	3.1	3.7
St. dev.	6.6	0.2	0.7	6.7	0.2	1.2	1.7

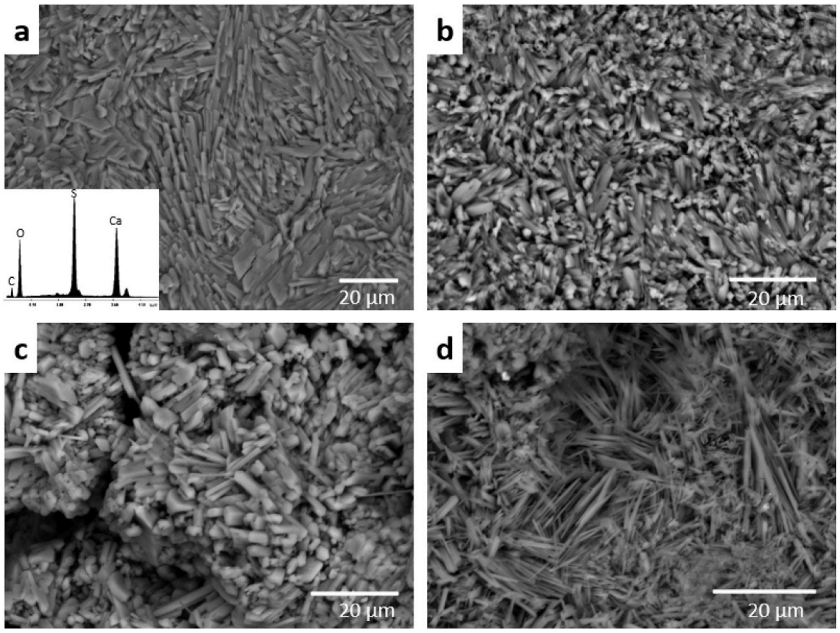

Fig. 11. Appearance of the samples' surface after the decay by sulfur dioxide. Tabular a) and prismatic b) gypsum crystals developed on the ghiara mortars and corresponding EDS spectrum; c) prismatic gypsum crystals and d) fibrous ettringite crystals formed on azolo mortars.

Results seem to be in contrast with the better mechanical performances previously ascertained by other authors for the ghiara mortars and ascribed to the higher reactive capability of ghiara when mixed with lime compared to azolo. This means that such reactivity positively influences the resistance of the mortar but only from a mechanical point of view, not in terms of chemical-physical durability. The latter is rather influenced by the microstructure of the material and particularly by its porosity and pore size distribution.

Author statement

All authors contributed to the study conception, once idealized by Cristina Maria Belfiore. Material preparation and data collection were performed by Cristina Maria Belfiore, Giada Montalto and Claudio Finocchiaro. Analyses were performed by Cristina Maria Belfiore, Giada Montalto and Paolo Mazzoleni. The first draft of the manuscript and its revised version were written by Cristina Maria Belfiore, Giada Montalto and Claudio Finocchiaro, with the supervision of Giuseppe Cultrone and Paolo Mazzoleni. All authors read and approved the final manuscript.

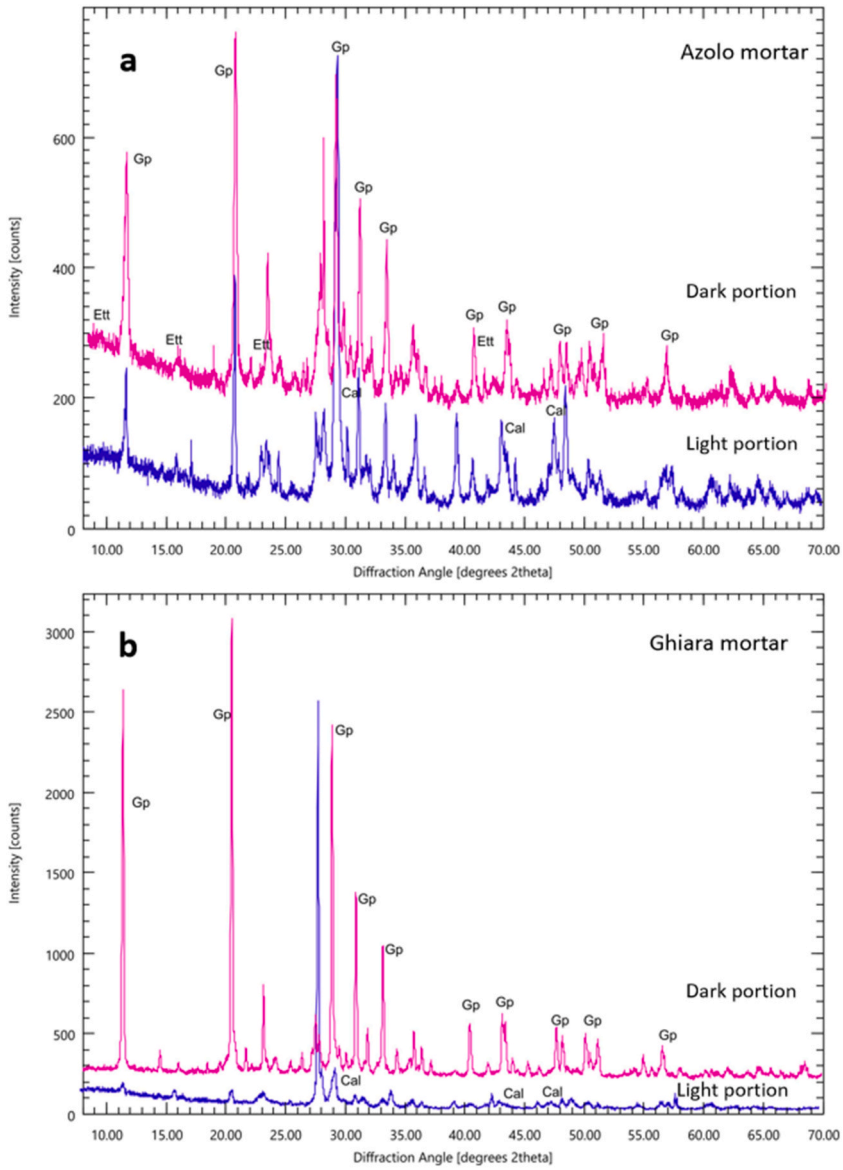

Fig. 12. XRD patterns obtained by the analysis carried out on a fragment of sample' surface after the SO_2 treatment: a) dark and light areas of azolo mortar; b) dark and light areas of ghiara mortar. Gp = gypsum; Cal = calcite; Ett = ettringite.

Declaration of competing interest

The authors declare that they have no known competing financial interests or personal relationships that could have appeared to influence the work reported in this paper.

Data availability

Data will be made available on request.

Acknowledgements

This research was financially supported by the PNRR project PE5 "CHANGES - Cultural Heritage Active Innovation for Sustainable Society" – Spoke 5 (CUP E63C22001960006), by the EU-funded PON REACT project (CUP E65F21002200005) and by the research group RNM 179 of the Junta de Andalucía (Spain).

Appendix A. Supplementary data

Supplementary data to this article can be found online at https://doi.org/10.1016/j.jobe.2023.108137.

References

[1] L. Anania, A. Badalà, G. Barone, C.M. Belfiore, C. Calabrò, M.F. La Russa, P. Mazzoleni, A. Pezzino, The stones in monumental masonry buildings of the "Val di Noto" area: new data on the relationships between petrographic characters and physical–mechanical properties, Construct. Build. Mater. 33 (2012) 122–132, https://doi.org/10.1016/J.CONBUILDMAT.2011.12.076.

[2] C.M. Belfiore, M.F. La Russa, A. Pezzino, E. Campani, A. Casoli, The Baroque monuments of Modica (Eastern Sicily): assessment of causes of chromatic alteration of stone building materials, Appl. Phys. Mater. Sci. Process 100 (2010) 835–844, https://doi.org/10.1007/S00339-010-5659-3/METRICS.

[3] C.M. Belfiore, G. Fichera, M.F. La Russa, A. Pezzino, The Baroque architecture of Scicli (south-eastern Sicily): characterization of degradation materials and testing of protective products, Period. Mineral. 81 (2012) 19–33, https://doi.org/10.2451/2012PM0002.

[4] C.M. Belfiore, C. Calabrò, S.A. Ruffolo, M. Ricca, Török, A. Pezzino, M.F. La Russa, The susceptibility to degradation of stone materials used in the built heritage of the Ortygia island (Syracuse, Italy): a laboratory study, Int. J. Rock Mech. Min. Sci. 146 (2021), 104877, https://doi.org/10.1016/J.IJRMMS.2021.104877.

[5] M.F. La Russa, G. Barone, C.M. Belfiore, P. Mazzoleni, A. Pezzino, Application of protective products to "Noto" calcarenite (south-eastern Sicily): a case study for the conservation of stone materials, Environ. Earth Sci. 62 (2011) 1263–1272, https://doi.org/10.1007/s12665-010-0614-3.

[6] M.F. La Russa, C.M. Belfiore, G.V. Fichera, R. Maniscalco, C. Calabrò, S.A. Ruffolo, A. Pezzino, The behaviour to weathering of the Hyblean limestone in the Baroque architecture of the Val di Noto (SE Sicily): an experimental study on the "calcare a lumachella" stone, Construct. Build. Mater. 77 (2015) 7–19, https://doi.org/10.1016/J.CONBUILDMAT.2014.11.073.

[7] R. Occhipinti, A. Stroscio, C. Maria, G. Barone, P. Mazzoleni, Chemical and colorimetric analysis for the characterization of degradation forms and surface colour modification of building stone materials, Construct. Build. Mater. 302 (2021), 124356, https://doi.org/10.1016/J.CONBUILDMAT.2021.124356.

[8] R. Punturo, L.G. Russo, A. Lo Giudice, P. Mazzoleni, A. Pezzino, Building stone employed in the historical monuments of Eastern Sicily (Italy). An example: the ancient city centre of Catania, Environ. Geol. 50 (2006) 156–169, https://doi.org/10.1007/S00254-006-0195-3/FIGURES/8.

[9] J.E. Prentice, Geology of Construction Materials, 1990. London.

[10] S. Branca, E. De Beni, C. Proietti, The large and destructive 1669 AD eruption at Etna volcano: reconstruction of the lava flow field evolution and effusion rate trend, Bull. Volcanol. 75 (2013) 694, https://doi.org/10.1007/s00445-013-0694-5.

[11] A. Piatanesi, S. Tinti, A Revision of the 1693 Eastern Sicily Earthquake and Tsunami, vol. 103, 1998, pp. 2749–2758.

[12] C.M. Belfiore, R. Visalli, G. Ortolano, G. Barone, P. Mazzoleni, A GIS-based image processing approach to investigate the hydraulic behavior of mortars induced by volcanic aggregates, Construct. Build. Mater. 342 (2022), 128063, https://doi.org/10.1016/J.CONBUILDMAT.2022.128063.

[13] S. Barbera, in: Recuper Catania, Gangemi Editor (Eds.), Tecniche Costruttive Dell'edilizia Etnea Nella Ricostruzione Settecentesca, 1998.

[14] G. Battiato, Le malte del centro storico di Catania, Mater. e Tec. Costr. Della Tradiz. Sicil. Doc. 16 Dell'Istituto Dipartimentale Di Archit, e Urban. Dell'Università Di Catania, 1988, pp. 85–107.

[15] C.M. Belfiore, M.F. La Russa, P. Mazzoleni, A. Pezzino, M. Viccaro, Technological study of "ghiara" mortars from the historical city centre of Catania (Eastern Sicily, Italy) and petro-chemical characterisation of raw materials, Environ. Earth Sci. 61 (2010) 995–1003, https://doi.org/10.1007/s12665-009-0418-5.

[16] G. Lanzafame, M.C. Caggiani, C. Finocchiaro, G. Barone, C. Ferlito, L. Gigli, P. Mazzoleni, Multidisciplinary characterization of the "Ghiara" volcanic paleosoil (Mt. Etna volcano, Italy): petrologic characters and genetic model, Lithos 418–419 (2022), 106679, https://doi.org/10.1016/J.LITHOS.2022.106679.

[17] C. Finocchiaro, C.M. Belfiore, G. Barone, P. Mazzoleni, IR-Thermography as a non-destructive tool to derive indirect information on the physical-mechanical behaviour of alkali activated materials, Ceram. Int. (2022), https://doi.org/10.1016/J.CERAMINT.2022.08.174.

[18] M. Thomson, J.-E. Lindqvist, J. Elsen, C. Groot, Porosity of historic mortars, in: 13th Int. Brick Block Mason, 2004.

[19] C. Groot, R. Veiga, I. Papayianni, R. Van Hees, M. Secco, J.I. Alvarez, P. Faria, M. Stefanidou, RILEM TC 277-LHS report: lime-based mortars for restoration–a review on long-term durability aspects and experience from practice, Mater. Struct. Constr. 55 (2022) 1–33, https://doi.org/10.1617/S11527-022-02052-1/FIGURES/19.

[20] I. Papayianni, J. Hughes, Testing properties governing the durability of lime-based repair mortars, RILEM Tech. Lett. 3 (2018) 135–139, https://doi.org/10.21809/RILEMTECHLETT.2018.81.

[21] C. Rispoli, A. De Bonis, V. Guarino, S.F. Graziano, C. Di Benedetto, R. Esposito, V. Morra, P. Cappelletti, The ancient pozzolanic mortars of the Thermal complex of Baia (Campi Flegrei, Italy), J. Cult. Herit. 40 (2019) 143–154, https://doi.org/10.1016/J.CULHER.2019.05.010.

[22] C. Rispoli, A. De Bonis, R. Esposito, S.F. Graziano, A. Langella, M. Mercurio, V. Morra, P. Cappelletti, Unveiling the secrets of roman craftsmanship: mortars from piscina mirabilis (Campi Flegrei, Italy), Archaeol. Anthropol. Sci. 12 (2020) 1–18, https://doi.org/10.1007/S12520-019-00964-8/FIGURES/13.

[23] C. Rispoli, S.F. Graziano, C. Di Benedetto, A. De Bonis, V. Guarino, R. Esposito, V. Morra, P. Cappelletti, New Insights of Historical Mortars Beyond Pompei: the Example of Villa del Pezzolo, Sorrento Peninsula, Miner 9 (2019) 575, https://doi.org/10.3390/MIN9100575, 9 (2019) 575.

[24] F. Izzo, A. Arizzi, P. Cappelletti, G. Cultrone, A. De Bonis, C. Germinario, S.F. Graziano, C. Grifa, V. Guarino, M. Mercurio, V. Morra, A. Langella, The art of building in the Roman period (89 B.C. - 79 A.D.): mortars, plasters and mosaic floors from ancient Stabiae (Naples, Italy), Construct. Build. Mater. 117 (2016) 129–143, https://doi.org/10.1016/j.conbuildmat.2016.04.101.

[25] A. Arizzi, H. Viles, I. Martín-Sanchez, G. Cultrone, Predicting the long-term durability of hemp–lime renders in inland and coastal areas using Mediterranean, Tropical and Semi-arid climatic simulations, Sci. Total Environ. 542 (2016) 757–770, https://doi.org/10.1016/J.SCITOTENV.2015.10.141.

[26] D. Gulotta, S. Goidanich, C. Tedeschi, L. Toniolo, Commercial NHL-containing mortars for the preservation of historical architecture. Part 2: durability to salt decay, Construct. Build. Mater. 96 (2015) 198–208, https://doi.org/10.1016/J.CONBUILDMAT.2015.08.006.

[27] P. Pineda, S. Medina-Carrasco, A. Iranzo, L. Borau, I. García-Jiménez, Pore structure and interdisciplinary analyses in Roman mortars: building techniques and durability factors identification, Construct. Build. Mater. 317 (2022), 125821, https://doi.org/10.1016/J.CONBUILDMAT.2021.125821.

[28] C. Borges, A. Santos Silva, R. Veiga, Durability of ancient lime mortars in humid environment, Construct. Build. Mater. 66 (2014) 606–620, https://doi.org/10.1016/J.CONBUILDMAT.2014.05.019.

[29] UNI-EN, 459-1:2015 Calci da costruzione - Parte 1: Definizioni, specifiche e criteri di conformità, 2015.

[30] A. Gueli, A. Lo Faro, A. Moschella, G. Stella, Un approccio multidisciplinare per la caratterizzazione del colore: un'applicazione sugli intonaci del centro storico di Catania, in: M. Editore (Ed.), Color. e Color. Contrib. Multidiscip., 2010, pp. 392–393.

[31] A. Altomare, C. Cuocci, C. Giacovazzo, A. Moliterni, R. Rizzi, QUALX: a computer program for qualitative analysis using powder diffraction data, J. Appl. Crystallogr. 41 (2008) 815–817, https://doi.org/10.1107/S0021889808016956.

[32] U. EN, UNI EN 1015-18:2004 Metodi di prova per malte per opere murarie - Determinazione del coefficiente di assorbimento d'acqua per capillarità della malta indurita, 2004.

[33] 12370 UNI-EN, Natural Stone Test Methods. Determination of Resistance to Salt Crystallization, 2020.

[34] C.M. Grossi, M. Murray, Characteristics of carbonate building stones that influence the dry deposition of acidic gases, Construct. Build. Mater. 13 (1999) 101–108, https://doi.org/10.1016/S0950-0618(99)00019-7.

[35] L. Tecer, Laboratory experiments on the investigation of the effects of sulphuric acid on the deterioration of carbonate stones and surface corrosion, Water. Air. Soil Pollut. 114 (1999) 1–12, https://doi.org/10.1023/A:1005177201808/METRICS.

[36] A.J. Lewry, D.J. Butlin, R.N. B, A chamber study of the effects of sulphur dioxide on calcareous stones, in: Proc. 7th Int. Congr. Deterior, . Conserv. Stone, Lisbon, 1992, pp. 641–650.

[37] J.B. Johnson, S.J. Haneef, B.J. Hepburn, A.J. Hutchinson, G.E. Thompson, G.C. Wood, Laboratory exposure systems to simulate atmospheric degradation of building stone under dry and wet deposition conditions, AtmEn 24 (1990) 2585–2592, https://doi.org/10.1016/0960-1686(90)90136-B.
[38] G. Fioretti, Ageing test e analisi di degrado di rocce carbonatiche pugliesi impiegate come pietre ornamentali e da costruzione, Università degli Studi di Bari Aldo Moro, 2016.
[39] G. Bultrini, I. Fragala, G.M. Ingo, G. Lanza, Minero-petrographic, thermal and microchemical investigation of historical mortars used in Catania (Sicily) during the XVII century A.D, Appl. Phys. Mater. Sci. Process 83 (2006) 529–536, https://doi.org/10.1007/s00339-006-3551-y.
[40] A. Arizzi, G. Cultrone, Mortars and plasters—how to characterise hydraulic mortars, Archaeol. Anthropol. Sci. 13 (2021) 1–22, https://doi.org/10.1007/S12520-021-01404-2/FIGURES/3.
[41] G. Mertens, P. Madau, D. Durinck, B. Blanpain, J. Elsen, Quantitative mineralogical analysis of hydraulic limes by X-ray diffraction, Cement Concr. Res. 37 (2007) 1524–1530, https://doi.org/10.1016/J.CEMCONRES.2007.08.002.
[42] I.G. Richardson, The calcium silicate hydrates, Cement Concr. Res. 38 (2008) 137–158, https://doi.org/10.1016/J.CEMCONRES.2007.11.005.
[43] M. Stefanidou, I. Papayianni, The role of aggregates on the structure and properties of lime mortars, Cem. Concr. Compos. 27 (2005) 914–919, https://doi.org/10.1016/J.CEMCONCOMP.2005.05.001.
[44] L. Falchi, U. Müller, P. Fontana, F.C. Izzo, E. Zendri, Influence and effectiveness of water-repellent admixtures on pozzolana–lime mortars for restoration application, Construct. Build. Mater. 49 (2013) 272–280, https://doi.org/10.1016/J.CONBUILDMAT.2013.08.030.
[45] B. Fitzner, R. Snethlage, Porosity properties and weathering behaviour of natural stones, GP News Lett 3 (1982).
[46] M. Angeli, D. Benavente, J.P. Bigas, B. Menéndez, R. Hébert, C. David, Modification of the porous network by salt crystallization in experimentally weathered sedimentary stones, Mater. Struct. Constr. 41 (2008) 1091–1108, https://doi.org/10.1617/S11527-007-9308-Z/FIGURES/13.
[47] G. Barone, P. Mazzoleni, G. Pappalardo, S. Raneri, Microtextural and microstructural influence on the changes of physical and mechanical proprieties related to salts crystallization weathering in natural building stones. The example of Sabucina stone (Sicily), Construct. Build. Mater. 95 (2015) 355–365, https://doi.org/10.1016/J.CONBUILDMAT.2015.07.131.
[48] A. Palomo, M.T. Blanco-Varela, S. Martinez-Ramirez, F. Puertas, C. Fortes, Historic Mortars: Characterization and Durability, New Tendencies for Research, Madrid, Spain, 2004.
[49] S.W. Mokrzycki, M. Tatol, Colour difference ΔE - a survey, Mach. Graph. Vis. Int. J. (2011), https://doi.org/10.5555/3166160.3166161.
[50] J. Peng, J. Zhang, J. Qu, Mechanism of the formation and transformation of ettringite, J. Wuhan Univ. Technol.-Materials Sci. Ed. 21 (2006) 158–161, https://doi.org/10.1007/BF02840908/METRICS.